Reactive Extrusion Processing of Polypropylene/TiO_2 Nanocomposites by In Situ Synthesis of the Nanofillers: Experiments and Modeling

Walid Bahloul
Laboratoire des Matériaux Polymères et Biomatériaux, UMR CNRS 5223, Ingénierie des Matériaux Polymères, Université de Lyon 1, 69622 Villeurbanne, France

Olivier Oddes
MINES ParisTech, Centre de Mise en Forme des Matériaux (CEMEF), UMR CNRS 1735, BP 207, 06904 Sophia Antipolis, France

Véronique Bounor-Legaré, Flavien Mélis, and Philippe Cassagnau
Laboratoire des Matériaux Polymères et Biomatériaux, UMR CNRS 5223, Ingénierie des Matériaux Polymères, Université de Lyon 1, 69622 Villeurbanne, France

Bruno Vergnes
MINES ParisTech, Centre de Mise en Forme des Matériaux (CEMEF), UMR CNRS 1735, BP 207, 06904 Sophia Antipolis, France

DOI 10.1002/aic.12425
Published online January 7, 2011 in Wiley Online Library (wileyonlinelibrary.com).

The effects of twin-screw extrusion processing conditions upon the formation of polypropylene/titanium dioxide (PP/TiO_2) nanocomposites are investigated. To prepare PP/TiO_2 nanocomposites by limiting the problem of filler dispersion at the nanoscale, an original method was developed based on the creation of TiO_2 through hydrolysis–condensation reactions (sol–gel method) of titanium n*-butoxide precursor during PP extrusion. The feed rate, the screw speed, and the amount of inorganic precursor were varied independently. The conversion rate of precursor as a function of process parameters was quantified by gas chromatography and mass spectroscopy combined techniques through the assessment of the alcohol formed. The effects of processing conditions on the development of the sol–gel reaction have also been investigated by using numerical simulations. The comparison between experimental and theoretical results shows that this simulation approach is relevant to predict the conversion of the inorganic precursor to TiO_2 through hydrolysis–condensation reactions in molten PP.*
 AIChE J, 57: 2174–2184, 2011
Keywords: polymer processing, simulation, process

Correspondence concerning this article should be addressed to B. Vergnes at bruno.vergnes@mines-paristech.fr.

Introduction

Organic/inorganic nanocomposite materials have attracted more and more attention for the last 10 years for their

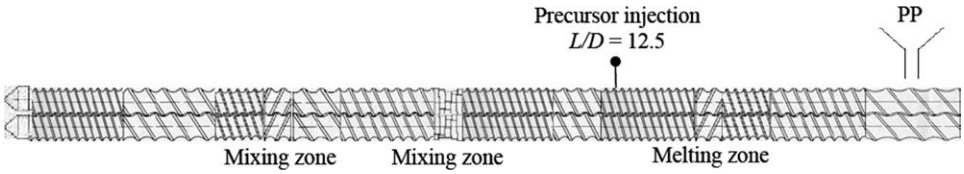

Figure 1. Screw profile and localization of injection point of titanium *n*-butoxide precursor.

special properties and industrial applications.[1–5] There are three principal procedures commonly used to disperse an inorganic phase in the organic matrix: dispersion in solution,[6,7] melt blending,[8–10] and in situ sol–gel processing.[11–13]

Nanocomposites materials obtained by melt blending have been intensively described.[14–19] In that case, melt processing conditions have an important influence on the nature and properties of the nanocomposite materials. However, because of the poor compatibility of hydrophilic nanoparticles with conventional hydrophobic polymer matrices such as polyolefins, nanodispersion is difficult to reach without particle agglomerations. Consequently, an original way to overcome these problems is the in situ synthesis of the inorganic filler in the molten polymer matrix by reactive extrusion. This synthesis is based on hydrolysis–condensation reactions (called classically ''sol–gel'') of silica or metal oxide precursors.[20] This approach has been largely developed for coating applications[21–23] allowing to create in mild conditions multifunctional organic–inorganic materials.

The transposition of this chemistry to the reactive extrusion consists of using an extruder (single or twin-screw) as a continuous chemical reactor.[24,25] In that case, besides the classical functions of a screw extruder (solid conveying, melting, mixing, and pumping), additional functions are involved, such as the development and the control of a chemical reaction (here, a sol–gel reaction). The main advantages of this approach are the following: compared to classical batch process in solution, the reaction is conducted in the melt, in the absence of a solvent, and it avoids the manipulation of nanoparticles. This makes this technique environmentally and economically favorable for industry. Numerous possible advantages in using reactive extrusion were described by Cassagnau et al.[26] and Vergnes and Berzin.[27]

However, there are some difficulties in using a reactive extrusion process: it is a complex process that involves many aspects, because of the high number of operating variables and their interactions during the process.[28] For example, molten polymers are generally non-Newtonian and their properties may change along the processing machine because of the chemical mixing and/or chemical reaction. The residence time, the pressure, mixing, and diffusion changes have to be known, these local flow conditions governing the reaction development, which will in turn modify the material properties (viscosity change and reaction exothermy), leading to change in bulk flow conditions. Finally, the extrusion of a viscous fluid is highly nonisothermal, and temperature changes have to be taken into account, because of heat transfer, viscous dissipation, and chemical reactions. Consequently, besides the traditional study of the chemical reaction mechanisms and kinetics, it is important to develop also theoretical approaches to provide useful tools to define the best conditions for conducting an operation of reactive extrusion and to control the process.

The main objective of this work is to demonstrate the potentiality of the reactive extrusion for synthesizing polypropylene/titanium dioxide (PP/TiO_2) nanocomposites. The effect of processing parameters, such as screw speed, feed rate, and concentration of inorganic precursor, upon the titanium *n*-butoxide hydrolysis–condensation reactions conversion will be investigated. Finally, from a prediction point of view, numerical simulations will allow us to better understand the relationships between processing parameters and conversion of titanium *n*-butoxide precursor.

Experimental

Materials

The system selected for the study is a polypropylene matrix and a titanium *n*-butoxide precursor ($Ti(OR)_4$). PP homopolymer (Moplen HP500N) was kindly supplied by LyondellBasell company. The zero-shear viscosity of this polymer is 4000 Pa s at 200°C. The titanium *n*-butoxide 97% from ABCR was used as titanium dioxide precursor, and the 2,6,10,15,19,23-hexamethyltetracosane (squalane, from Aldrich) was selected as a PP model medium.

Extrusion conditions and characterization techniques

The nanocomposite materials were prepared using a corotating twin-screw extruder (Leistritz LSM 30-34, screw diameter $D = 34$ mm and length to diameter ratio $L/D = 34.5$). A specific screw profile, as shown in Figure 1, was designed for the in situ synthesis of TiO_2 in the molten PP matrix. It is composed of right-handed screw elements (conveying zone), a left-handed element for the PP melting before titanium *n*-butoxide injection, and two successive mixing zones, one with a kneading block of five discs staggered at 30° and a second one with a left-handed element, situated before the die exit. The liquid precursor was continuously injected at a constant flow rate from a side feeder and added to molten PP after the melting zone (point at $L/D = 12.5$) using a HPLC pump. For example, for 3 kg h^{-1} and 10% of precursor, the flow rate was 6.8 mL min^{-1}. It is important to point out that, in these experiments, no water was added during extrusion process. The hydrolysis–condensation reactions were initiated thanks to the water contained in surrounding humidity. The extruder barrel was divided into 10 equal zones, each one provided with individual temperature control system. The barrel temperature was fixed at 200°C for all experiments. The processing parameters studied were the feed rate Q, the screw speed N, and the titanium *n*-butoxide concentration [$Ti(OR)_4$], which were varied independently: $Q = 1$, 3, and 5 kg h^{-1}, $N = 150$, 200, and 300 rpm, and [$Ti(OR)_4$] = 10, 20, and 30 wt %.

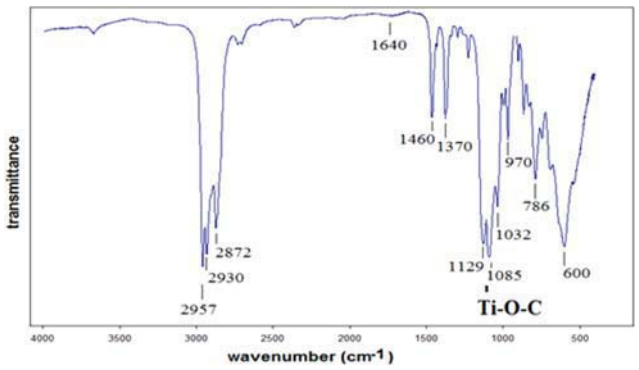

Figure 2. FTIR spectrum of titanium *n*-butoxide precursor.

[Color figure can be viewed in the online issue, which is available at www.wileyonlinelibrary.com.]

For each extrusion condition, samples were collected at die exit for characterizing reaction conversion, filler morphology, and rheological properties. The conversion resulting from hydrolysis–condensation reactions at the die exit was evaluated by measuring the quantity of residual butanol (butanol from nonreacted butoxide groups or butanol embedded in the polymer matrix) in the extruded samples by using TGA-GC-MS experiments. TGA-GC-MS is a coupling technique based on thermal gravimetry (TGA), gas chromatography (GC), and mass spectroscopy (MS) allowing identification of the byproducts and specifically, in the present case, the assessment of the residual butanol. The inorganic TiO_2 contents obtained from TGA measurement (the residual mass after pyrolysis at 400°C) correlate quite well with conversion rate values calculated from TGA-GC-MS experiments.

The TGA experiments were performed with a TA Q600 from TA Instruments. All the experiments were carried out both under an inert nitrogen atmosphere and under oxidative working conditions (air) at a flow rate of 50 mL min^{-1}. Samples were heated from room temperature up to 450°C with a heating rate of 100°C min^{-1}. The released volatiles were transferred on-line (constant feed rate and pressure) to a gas chromatograph Agilent 6890N equipped with a 19091 S 433 columns and a mass spectrometer Agilent MS 5973N detector (mass range *m*/*z* 10–700).

FTIR spectra were obtained from a thin layer (200 μm) of sample (titanium *n*-butoxide diluted or not in squalane) exposed to surrounding humidity. Measurements were conducted with a KBr windows enclosed in a heating cell. The FTIR spectra were recorded with a resolution of 1 cm^{-1} and with 32 scans on a Magna-IR™ Spectrometer 550.

Chemistry and kinetics of hydrolysis–condensation reactions

The formation of TiO_2 particles results from the hydrolysis and condensation reactions as follows:Hydrolysis of inorganic precursor leads to the formation of Ti—OH groups:

$$Ti(OR)_4 + H_2O \rightleftharpoons Ti(OR)_3OH + ROH \quad (1)$$

The condensation of two Ti—OH groups via oxolation or one Ti—OH with Ti—OR via alcoxalation, represented by the two following reactions, leads to the formation of oxo bridges Ti—O—Ti:

Oxalation (or water elimination):

$$Ti(OR)_3OH + Ti(OR_3)OH \rightleftharpoons (OR)_3—Ti—O—Ti—(OR)_3 + H_2O \quad (2)$$

Alcoxalation (or alcohol elimination):

$$Ti(OR)_3OH + Ti(OR)_4 \rightleftharpoons (OR)_3—Ti—O—Ti—(OR)_3 + ROH \quad (32)$$

However, it is very difficult to differentiate these two steps.

In a previous work, the characterization of this reactional medium has been made with a model medium made of titanium *n*-butoxide at different concentrations and dispersed in squalane at different temperatures (Bahloul et al., submitted). Squalane was selected to study the influence of a nonpolar medium on the titanium *n*-butoxide hydrolysis–condensations reactions kinetics. Experiments were conducted at constant temperature, directly in the FTIR cell, after mixing of squalane with precursor. The progress of the reaction has been followed by infrared measurements (FTIR) from the evolution of the area of the Ti—O—C band (Figure 2) as a function of reaction time. The area corresponding to Ti—O—C concentration at $t = 0$ was denoted A_0. The same area for a reaction time t (min) will be noted A_t. The conversion p (expressed in %) corresponding to the disappearance of Ti—O—C bonds was calculated according to the following equation:

$$p = \left(1 - \frac{A_t}{A_0}\right) \times 100. \quad (4)$$

From these experimental results, various kinetic orders have been tested. Best fits with linear variations were obtained by plotting $\ln p = f(t)$ in accordance with a global first-order reaction. The kinetic constants at different temperatures are reported in Table 1. For the following, we will assume that these kinetic data, determined in a liquid model medium, remain valid in the molten PP. It could seem a strong assumption, but the results will show that it must be not so far from reality.

However, for the further simulation, we must define kinetic equations on a wide range of temperatures, typically from 170 to 300°C. These equations have to fit at best the

Table 1. Experimental Reaction Rate Constants at Different Temperatures and Activation Energies for Different Precursor Concentrations in Squalane Medium

	k (min^{-1}) 180°C	k (min^{-1}) 220°C	k (min^{-1}) 250°C	E (kJ mol^{-1})
Pure titanium *n*-butoxide	0.29	0.50	0.83	47
10 wt % $Ti(OR)_4$	0.10	0.61	0.91	65
20 wt % $Ti(OR)_4$	0.07	0.37	0.75	66
30 wt % $Ti(OR)_4$	0.05	0.28	0.87	79

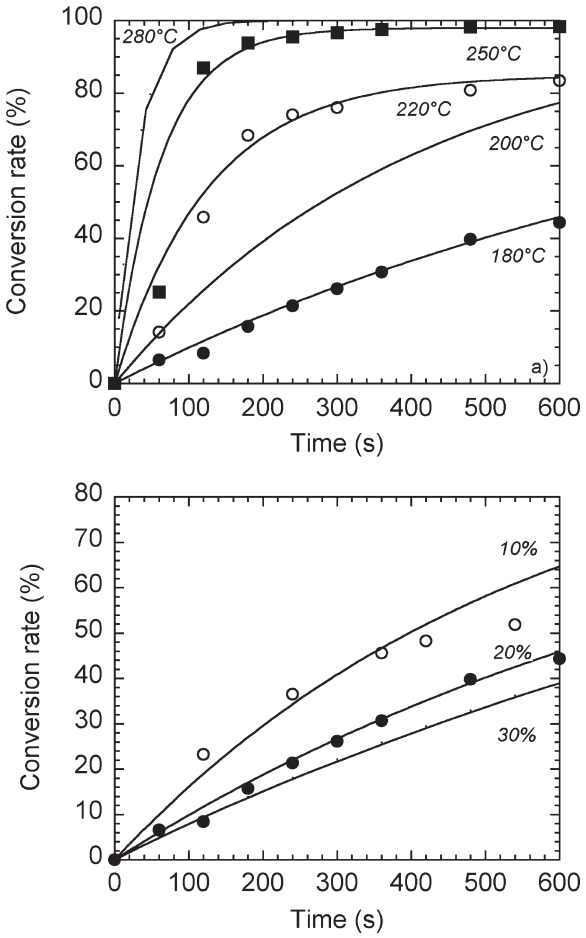

Figure 3. Variation of conversion rate vs. time (a) at different temperatures (20 wt % inorganic precursor) and (b) at different inorganic precursor amounts (180°C).

Symbols are experimental values measured by infrared spectroscopy. Full lines are theoretical prediction with Eq. 5.

experimental kinetics, but on a time domain much shorter than the experimental one. Experimental kinetics was monitored for 1 h, whereas the residence times in the extruder are of the order of a few minutes. Consequently, we will define the kinetic laws between 0 and 600 s. We will choose for the conversion the following expression:

$$\chi = \chi_\infty[1 - \exp(-kt)], \tag{5}$$

where χ_∞ is the maximum conversion and k is the kinetic constant following Arrhenius law:

$$k = k_0 \exp\left(-\frac{E}{RT}\right), \tag{6}$$

where k_0 is the pre-exponential factor, E is the activation energy, R is the gas constant, and T is the absolute temperature.

Figure 3a shows the good agreement between experimental and calculated conversion values. At high temperatures, high conversion rates can be obtained within few minutes, which is the order of magnitude of residence times in extrusion. Furthermore, the model allows us to extrapolate conversion data at high temperatures, possibly encountered during the process, but for which experimental data would be quite impossible to obtain. Figure 3b shows that the kinetics is slower when the inorganic precursor amount increases, what could also been deduced from the experimental kinetic constants in Table 1.

Modeling

The objective of this part of the study was to develop a global model to describe the development of the sol–gel reaction of titanium *n*-butoxide along the extruder. For that, it is necessary to have access to the local flow conditions and to know the reaction kinetics. For the knowledge of local flow conditions, we have used the software Ludovic©.[29] This software has been developed by Vergnes et al.[29] more than 10 years ago. Based on a 1D approach of continuum mechanics, it allows us, by solving mass balance and heat transfer equations, to calculate the evolution along the screws of the main parameters of the extrusion process (among which pressure, temperature, residence time, shear rate, and filling ratio). Computations are done separately for each type of element (partially or totally filled right-handed screw elements, left-handed screw elements, and blocks of kneading discs). For screw elements, pressure/flow rate relationships are calculated assuming a rectangular channel cross section with constant width and taking into account side effects using correcting factors. For flow in kneading blocks, we consider the peripheral flow around each individual disc, characterized by a pressure peak located before the disc tip. The staggering of the tips of adjacent discs induces a staggering of the pressure profiles, creating thus an axial pressure gradient pushing the material in the axial direction. The preceding elementary models are linked together to obtain a global description of the flow field along the extruder. After defining screw profile, barrel geometry, polymer characteristics (thermal parameters, density, and viscosity as a function of shear rate and temperature), and operating conditions (feed rate, screw speed, and barrel thermal regulation), the software provides the local values of thermal and mechanical flow parameters including residence time distribution. This software has been validated through comparisons with experiments[30] and largely used for many applications, such as compounding of polymer blends[31] and composites.[32]

Regarding hydrolysis–condensation reactions, we consider a global kinetics described by a first-order model (Eqs. 5 and 6), including both reactions of hydrolysis and condensation. Then, by coupling the thermomechanical model with the kinetic equations, it is possible to calculate the progress of the conversion all along the screws.[27]

Once again, Ludovic© has been largely used in the past to calculate different operations of reactive extrusion, including controlled polymer degradation,[33] polymerization reaction,[34] or polymer chemical modifications.[35,36] In the present case, we consider that the formation of nanofillers does not modify the rheological behavior of the matrix. Actually, the influence of nanofillers on the rheological behavior of nanocomposites is mainly observed at low frequency.[37] In the range of shear rates encountered in extrusion (typically, 1–500 s^{-1}), we can consider this effect as negligible.

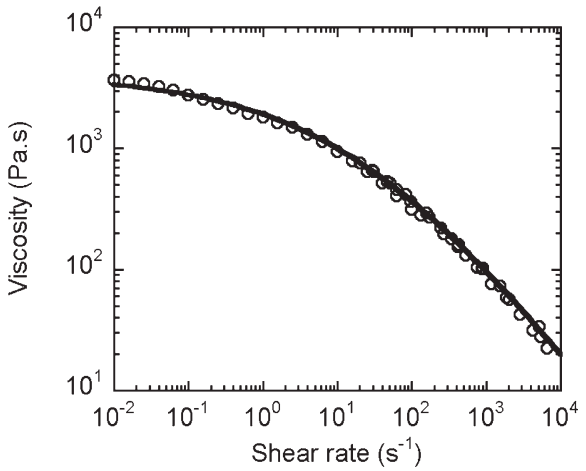

Figure 4. Master curve of the PP shear viscosity at 200°C.

The full line is the fit by the Carreau–Yasuda model.

Consequently, we will assume that the material has the viscosity of the PP matrix. It is predicted by Carreau–Yasuda law[38] (Figure 4):

$$\eta = \eta_0 a_T (1 + (\lambda \dot{\gamma} a_T)^a)^{\frac{m-1}{a}}, \tag{7}$$

where $\dot{\gamma}$ is the shear rate, η_0 is the zero-shear viscosity, λ is a characteristic time, a is the Yasuda parameter, and m is the power law index.

η_0 and λ vary with temperature, according to Arrhenius law, defined by the parameter a_T:

$$a_T = \exp\left(\frac{E}{R}\left(\frac{1}{T} - \frac{1}{T_0}\right)\right), \tag{8}$$

where E is an activation energy, R is the gas constant, and T_0 is the reference temperature. For the selected PP, we have obtained the following values: $\eta_0 = 4000$ Pa s, $a = 0.32$, $\lambda = 0.05$ s, $E = 46$ kJ mol^{-1}, $m = 0.29$, and $T_0 = 200$°C. As shown in Figure 4, this law permits an accurate description of the viscosity over six orders of magnitude of shear rates.

To obtain the conversion rate, we calculate in a first step the flow conditions into the extruder, with the rheological law proposed above (Eqs. 7 and 8). Then, from the computed values of local temperature and residence time, the conversion rate is computed using Eqs. 5 and 6.

Results and Discussion

In this section, we will present in parallel the experimental results and the interpretations supported by the modeling. Actually, to better interpret the influence of the process parameters on the chemical reaction and the final conversion, we have studied the various extrusion experiments that have been performed at different feed rates ($Q = 1$, 3, and 5 kg h^{-1}), screw speeds ($N = 150$, 200, and 300 rpm), and inorganic precursor concentrations (10, 20, and 30 wt %).

First of all, we must check the obtained morphology. TEM micrographs clearly show particles of TiO_2, with a diameter of a few tens of nanometers, homogeneously distributed in the PP matrix (Figure 5).

During extrusion experiments, it has been shown that the die pressure evolution with flow rate was different according to the inorganic precursor amount (Figure 6). As the product temperature was similar at the same flow rate, this can only be explained by a reduction in the viscosity with the amount of precursor, probably because of a dilution effect when a large quantity of very low viscous material is introduced in the molten PP matrix. This has been taken into account in the modeling by decreasing the zero-shear viscosity using a mixing law:

$$\eta_0 = \eta_{0\,\mathrm{prec}}\,[\mathrm{Ti(OR)_4}] + \eta_{0\,\mathrm{PP}}\left(1 - [\mathrm{Ti(OR)_4}]\right), \tag{9}$$

where $[Ti(OR)_4]$ is the inorganic precursor concentration (in wt %), $\eta_{0\,\mathrm{PP}}$ is the zero-shear viscosity of PP, and $\eta_{0\,\mathrm{prec}}$ is one of the inorganic precursors. We obtained 3200 and 2800 Pa s for 20 and 30 wt % inorganic precursors, respectively.

As we will see in more details later on, the variations of conversion as a function of feed rate, screw speed, and

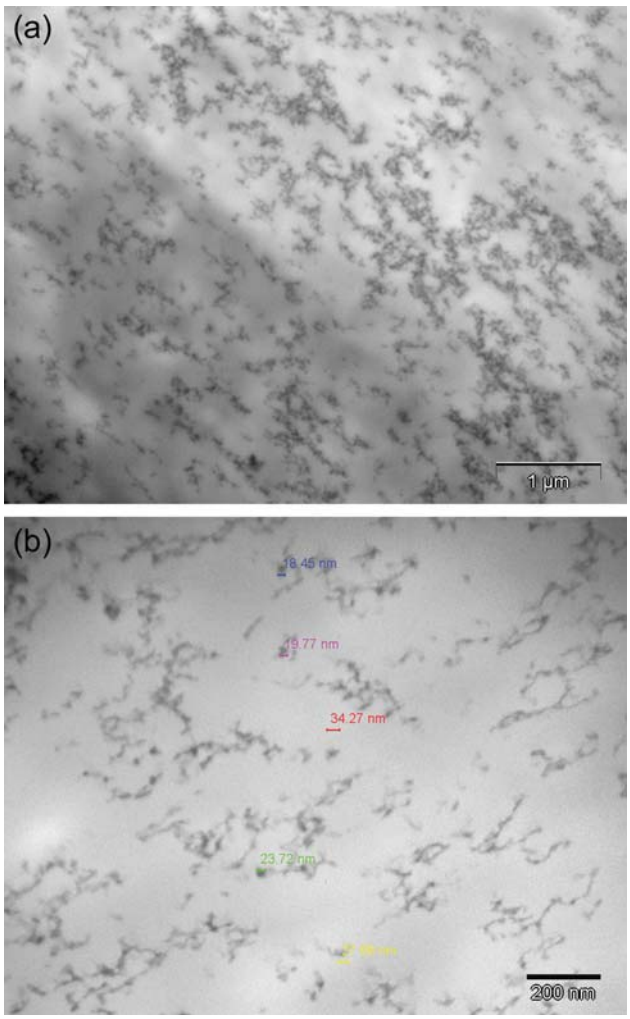

Figure 5. TEM micrographs of an extruded sample (5 kg h^{-1}, 150 rpm, and 20 wt % inorganic precursor).

(a) Bar scale: 1 μm and (b) bar scale: 200 nm. [Color figure can be viewed in the online issue, which is available at www.wileyonlinelibrary.com.]

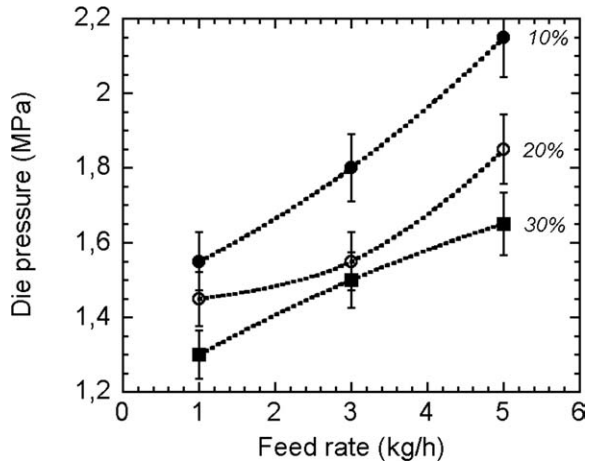

Figure 6. Variation of experimental die pressure vs. feed rate for different inorganic precursor amounts (150 rpm).

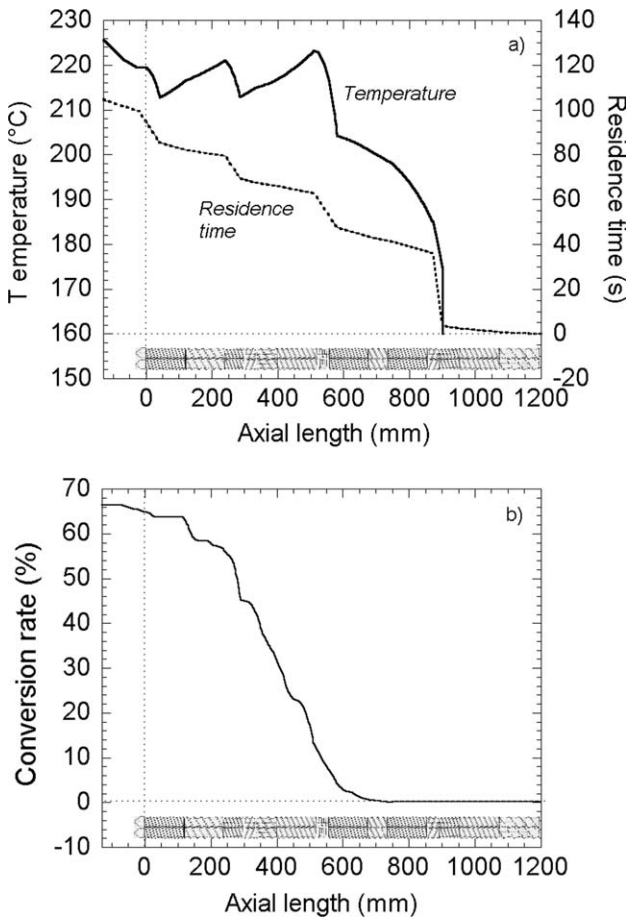

Figure 7. Ludovic© modeling results for sample prepared at 150 rpm, 5 kg h^{-1}, and 30 wt % of inorganic precursor.

(a) Evolution of temperature and cumulative residence time along the screws and (b) evolution of conversion rate along the screws.

amount of precursor can be principally explained in terms of residence time and melt temperature inside the extruder.

Figure 7 shows an example of results provided by Ludovic© simulation. Figure 7a presents the evolution of temperature and cumulative residence time for the following processing conditions: 5 kg h^{-1}, 150 rpm, and 30 wt % of inorganic precursor. The temperature increases rapidly from the melting section (first left-handed element) to the die exit. It varies depending on the screw profile: in the restrictive elements (left-handed elements, kneading discs), it increases rapidly by viscous dissipation. In the screw conveying elements, where the viscous dissipation is negligible, temperature decreases by heat transfer toward the barrel at a lower temperature (here, 200°C). At the die exit, the melt temperature is around 225°C. The residence time increases mainly in the filled sections of the screw profile (restrictive elements and die). For these processing conditions, the total residence time is around 104 s.

Then, from the local values of residence time and temperature, it is now possible by using Eqs. 5 and 6 to calculate the evolution of conversion all along the screws. It is shown in Figure 7b: conversion increases regularly along the screws, from the injection point of the inorganic precursor (axial location: $z = 765$ mm. Axis origin is at the junction between die and extruder). Finally, the conversion extent reaches a plateau at the end of the screws. This final calculated conversion is close to 67% in this case.

Influence of feed rate

As modeling allows us to obtain information on the evolution of the flow variables, we have used it to explain the influence of control parameters (feed rate, screw speed, and inorganic precursor amount) that we have observed in the experiments. Figure 8 shows the effect of flow rate on experimental conversion rate at the die exit for different screw speeds for 20 wt % of precursor (similar results were obtained for other inorganic precursor amounts). For each screw speed, conversion decreases when flow rate is increased. Figure 9 shows the results of the modeling for

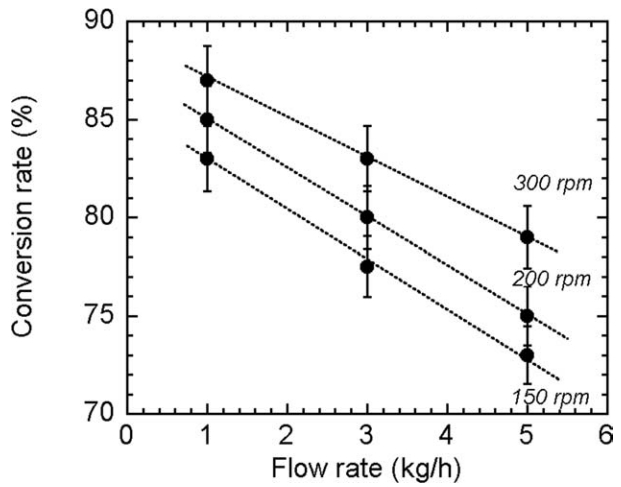

Figure 8. Experimental conversion rate as a function of flow rate for different screw speeds at 20 wt % of inorganic precursor.

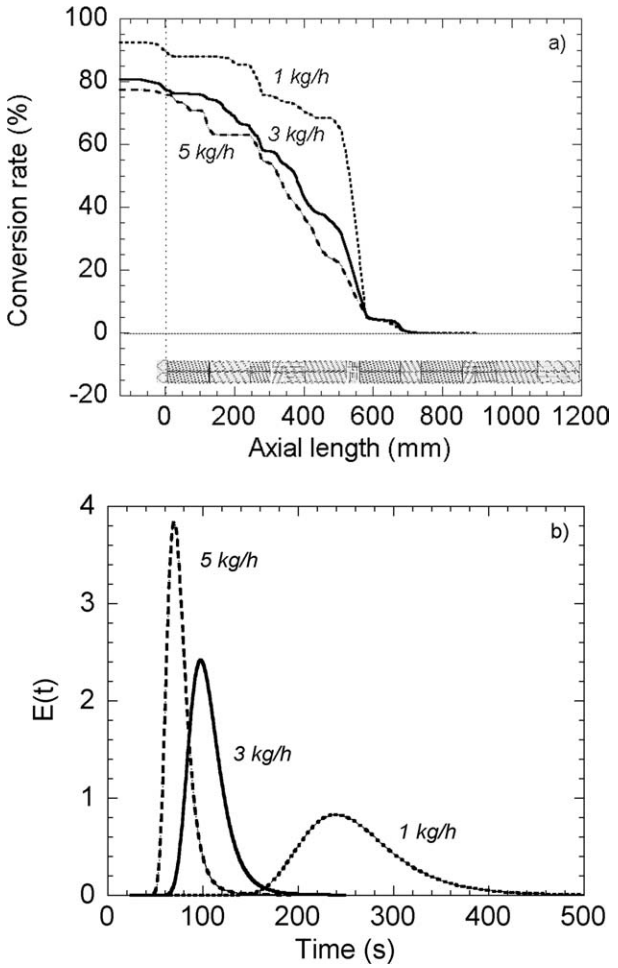

Figure 9. (a) Evolution along the screws of conversion rate as a function of feed rate (N = 200 rpm, 10 wt % of inorganic precursor).

(b) Evolution of residence time distribution with the feed rate (N = 200 rpm, 10 wt % of inorganic precursor).

10 wt % of precursor and a screw speed of 200 rpm. We observe effectively that the conversion decreases when the feed rate is increased, in agreement with experimental observations. The calculated conversion rate at die exit is 93, 81, and 78% for 1, 3, and 5 kg h^{-1}, respectively. This effect can be essentially explained by the reduction of residence time. Indeed, the temperature is slightly affected by the flow rate. Final calculated temperature was 234, 234, and 233°C for 1, 3, and 5 kg h^{-1}, respectively. On the contrary, as it can be seen in Figure 9b, residence time distribution is greatly modified when feed rate is changed. An increase in feed rate from 1 to 5 kg h^{-1} induces a reduction of the mean residence time from 243 to 71 s and a narrowing of the distribution (the variance of the distribution varies from 4930 to 370 s^2). Consequently, the reaction time is shorter, which results to a lower conversion. In fact, the residence time in the extruder is one of the most important parameters (the temperature is another one) governing the chemical reaction evolution. Calculated values of final temperature and residence time are given in Table 2. It can be seen in Figure 10 from comparison with experimental values (10 wt % of inorganic precursor, 200 rpm) that the order of magnitude and the tendency of the modeled values are correctly described.

Table 2. Calculated Values of Final Temperatures and Residence Time for Various Processing Conditions

Screw Speed N (rpm)	Feed Rate Q (kg h^{-1})	Precursor Amount (wt %)	Final Temperature (°C)	Mean Residence Time (s)
150	1	10	226	253
150	3	10	226	104
150	5	10	225	80
200	1	10	234	243
200	3	10	234	100
200	5	10	233	71
300	1	10	250	239
300	3	10	250	90
300	5	10	250	62
150	3	20	223	110
200	3	20	234	102
300	3	20	250	92
150	3	30	225	112
200	3	30	234	103
300	3	30	250	94

Influence of screw speed

The changes in conversion rate with screw speed can also be seen in Figure 8: typically, for any flow rate, conversion increases with screw speed. The influence of screw speed at a constant feed rate of 1 kg h^{-1} at 10 wt % of inorganic precursor is indicated in Figure 11a. We observe a slight increase of the conversion with the screw speed, similar to the one obtained experimentally (Figure 11b). In this case, it can be explained by the fact that, when screw speed is increased, the residence time is slightly reduced, when the temperature is increased by viscous dissipation: in the present case, the exit temperature is, respectively, 226, 234, and 250°C for 150, 200, and 300 rpm (see Table 2). Consequently, the reaction is faster (see Figure 4a) and, even though the time is shorter, the conversion is higher. However, if we consider now the case at 5 kg h^{-1} for 10 wt %

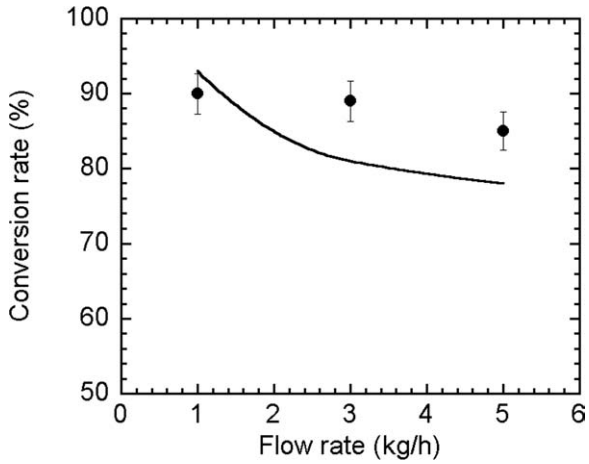

Figure 10. Comparison between experimental (symbols) and computed (full line) values of conversion rate at the die exit (N = 200 rpm, 10 wt % of inorganic precursor).

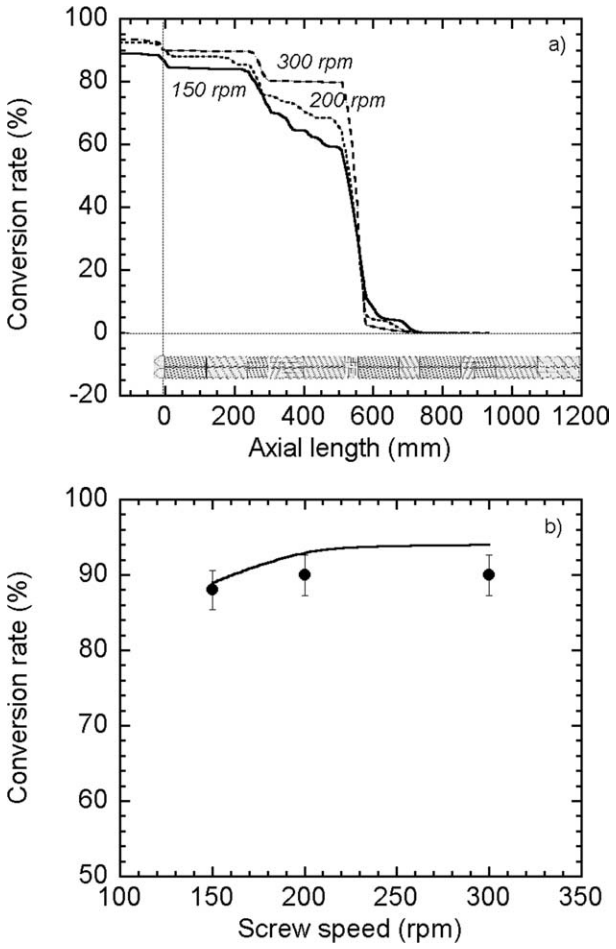

Figure 11. Evolution of conversion rate as a function of screw speed (Q = 1 kg h^{-1}, 10 wt % of inorganic precursor).

(a) Along the screws and (b) at the die exit: comparison between experimental (symbols) and computed (full line) values.

of inorganic precursor, we can see in Figure 12a that the ranking of the curves is no more monotonous: the maximum value of conversion (82%) is now obtained at 150 rpm. Lower values are calculated for the other speeds, respectively, 78% at 200 rpm and 81% at 300 rpm. Once again, these tendencies are perfectly in agreement with the experiments (Figure 12b). In these conditions, the feed rate is high and, consequently, the residence time is shorter (see Figure 9b and Table 2). When the screw speed is increased from 150 to 200 rpm, residence time decreases from 80 to 71 s but, at the same time, there is an increase in temperature from 225 to 233°C, related to viscous heating. In this case, time reduction (−9 s) is preponderant compared with temperature increase (+8°C). However, for the next increase between 200 and 300 rpm, the gap in temperature (from 233 to 250°C) becomes now more important that the decrease of residence time (from 71 to 62 s). Consequently, the conversion increases again. Contrary to the feed rate influence, a change in screw speed can thus create effects that are opposite in nature, according to chosen processing conditions.

Influence of inorganic precursor concentration

Finally, we tested the influence of the precursor amount. Figure 13 shows that, whatever the processing conditions, the measured conversion rate decreases when the inorganic precursor amount increases. This is due to the fact that the kinetics is slower at high precursor amount (see Figure 4b). However, the calculated filler content is more important at high precursor amount, despite the lower conversion (Figure 13b). The filler content (in wt %) is evaluated from conversion rate resulting from hydrolysis–condensation reactions (χ) and initial weight percentage of inorganic precursor introduced in the extruder ([Ti(OR)$_4$]) according to:

$$[\text{filler}] = \frac{\chi[\text{Ti(OR)}_4]0.3}{\chi[\text{Ti(OR)}_4]0.3 + (1 - [\text{Ti(OR)}_4])} \times 100, \quad (10)$$

where 0.3 corresponds to the molar mass ratio between the initial [Ti(OR)$_4$] and the final [TiO$_2$] in case of complete conversion of the hydrolysis–condensation reactions.

We can also observe different effects of screw speed as a function of precursor amount: for 10 wt %, conversion rate

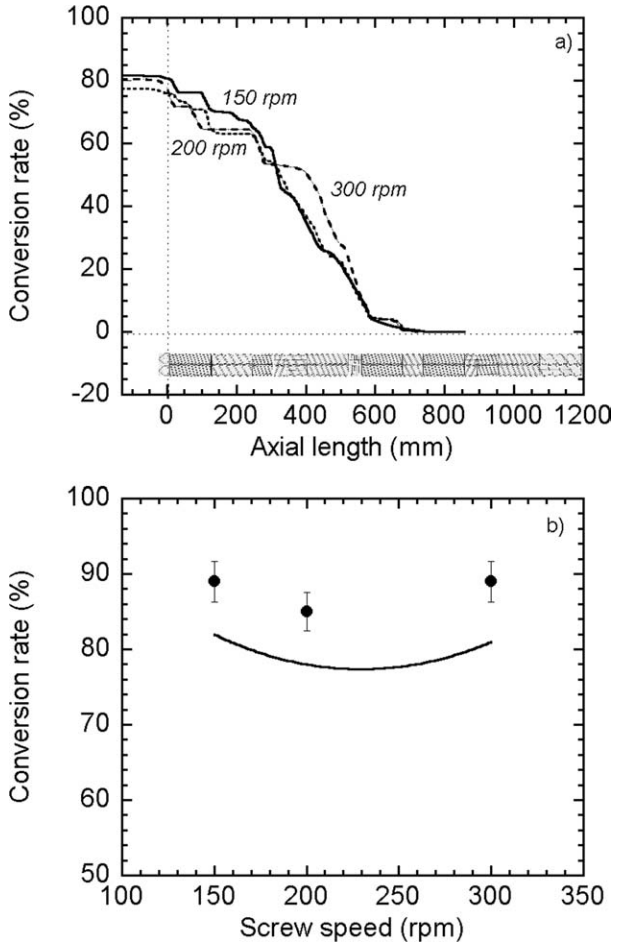

Figure 12. Evolution of conversion rate as a function of screw speed (Q = 5 kg h^{-1}, 10 wt % of inorganic precursor).

(a) Along the screws and (b) at the die exit: comparison between experimental (symbols) and computed (full line) values.

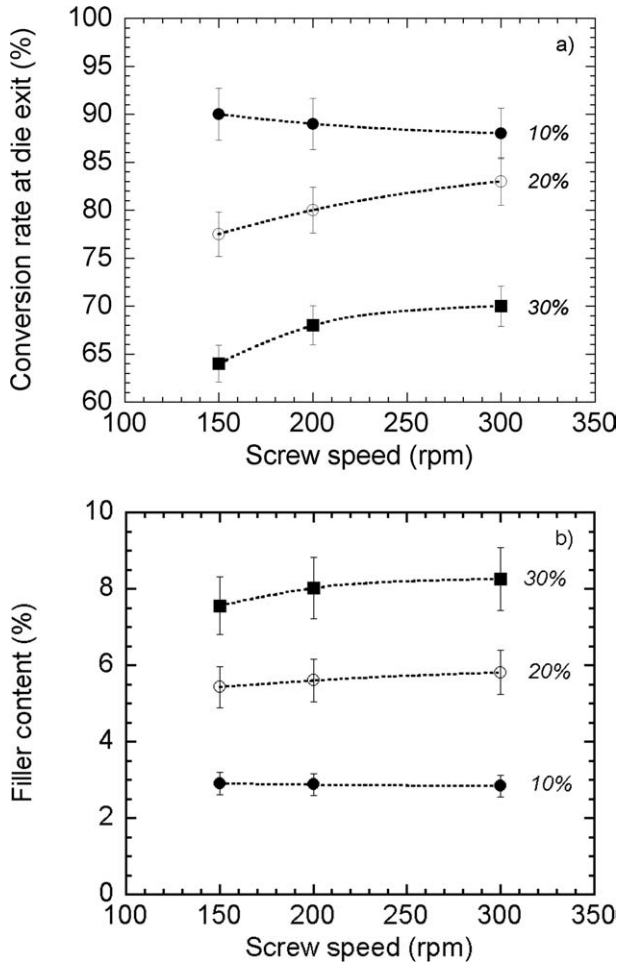

Figure 13. (a) Experimental conversion rate and (b) inorganic TiO_2 synthesized content vs. screw speed for different inorganic precursor concentrations at $Q = 3$ kg h^{-1}.

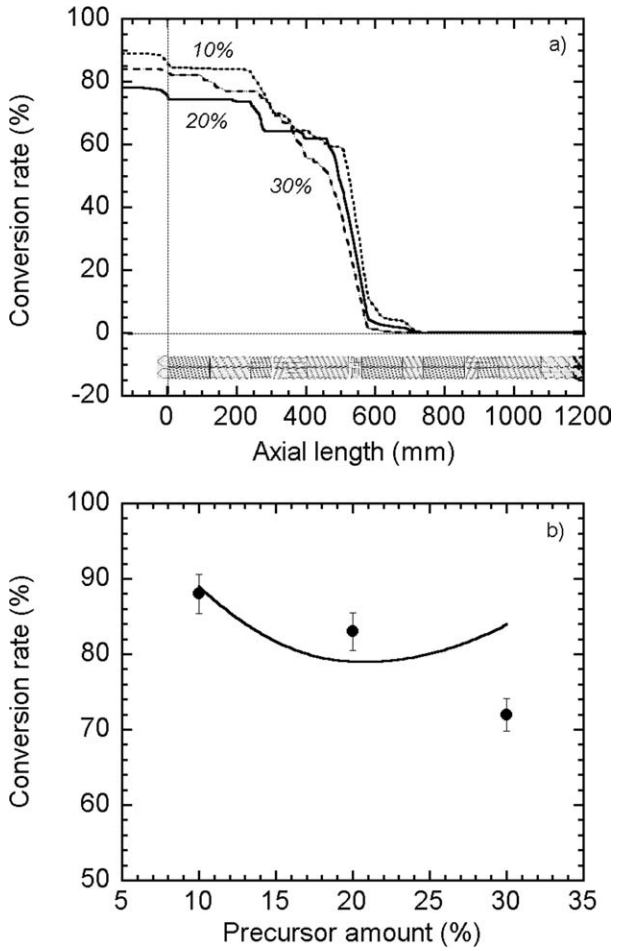

Figure 14. Evolution of conversion rate as a function of inorganic precursor concentration ($Q = 1$ kg h^{-1}, $N = 150$ rpm).

(a) Along the screws and (b) at the die exit: comparison between experimental (symbols) and computed (full line) values.

slightly decreases with screw speed, whereas it increases for 20 and 30 wt %. It is shown in Figure 14a that, at 1 kg h^{-1} and 150 rpm, the calculated conversion is maximum for 10 wt % (89%), then decreases for 20 wt % (to 79%) before to increase again for 30 wt % (84%). In the experiments, we only observe a continuous decrease with increase in precursor amount (Figure 14b). In this case, it seems that the theoretical predictions for 30 wt % of inorganic precursor are not correct. In fact, at high precursor amount, the assumption made on the rheological behavior is probably not valid, because the reactional medium may be heterogeneous. Indeed, the mixing of a low viscosity liquid (high amount of inorganic precursor) with a molten polymer leads to highly nonlinear phenomena as lubrication effects, associated with complex flow patterns, and diffusion mixing occurs. The large difference between the inorganic precursor viscosity and that of the molten polymer greatly magnifies the difficulties associated with homogenizing these components in a laminar flow. Another possible reason for the unsatisfactory results at 30% can be an inaccurate kinetic equation, because experimental characterizations were much more difficult to carry out at high precursor content.

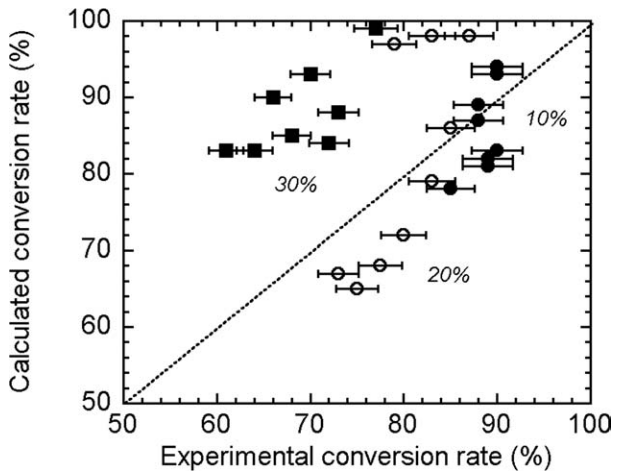

Figure 15. General comparison between experimental and computed conversion rates.

Finally, to completely validate the actual model, we have compared all the experimental results with the calculations for 10, 20, and 30 wt % inorganic precursor. Results are shown in Figure 15 for the various feed rates and screw speeds. It is clearly shown that the prediction for 10 and 20 wt % is satisfactory, leading to a correct value of the conversion rate at $\pm 15\%$, irrespective of screw speed and feed rate. However, the calculations at 30 wt % provide overestimation of the conversion. It confirms that the model does not work in this particular condition, probably, as previously explained, because of an inaccurate characterization of the kinetic data or heterogeneous conditions for the reaction.

Conclusion

In this work, PP/TiO2 nanocomposites were prepared from the hydrolysis–condensation reactions (sol–gel method) of titanium *n*-butoxide (inorganic precursor) during PP processing in a twin-screw extruder. We have studied, from experimental and simulation points of view, the influence of processing conditions (feed rate, screw speed, and inorganic precursor amount) on the inorganic precursor conversion at the die exit. We have shown the potentiality of a theoretical model (based on 1D simulation) to describe the preparation of these nanocomposites by reactive extrusion. Based on a kinetic equation and a thermomechanical solver, the model permits to predict the evolution of the hydrolysis–condensations reactions along the screws for different processing conditions. A comparison with experiments shows that the orders of magnitude and the influence of processing parameters (screw speed and feed rate) are correctly described for most of the processing conditions by the simulation. However, at high concentration of inorganic precursor (30 wt %), the simulation overestimates the experimental values. One possible explanation of this disagreement is a lubricant effect of the inorganic precursor leading to nonhomogeneous conditions for the sol–gel process or an inaccurate characterization of the kinetic data. Finally, our work confirms that the preparation of PP/TiO_2 nanocomposites by in situ method can be achieved by a reactive process in a twin-screw extruder. In parallel, the use of a simulation software, developed for reactive extrusion applications, allowed us to better understand and control this reactive process.

Acknowledgments

This study was carried out in the frame of the European Research Program "Multihybrids," in the 6th PCRD Program.

Literature Cited

1. Innocenzi P, Brusatin G. Fullerene-based organic-inorganic nanocomposites and their applications. *Chem Mater*. 2001;13:3126–3139.
2. Interrante LV. Editorial: special issue on nanostructured materials. *Chem Mater*. 1995;7:1751–1752.
3. Komarneni S. Nanocomposites. *J Mater Chem*. 1992;2:1219–1230.
4. Gleiter H. Nanostructured materials. *Adv Mater*. 1992;4:474–481.
5. Novak BM. Hybrid nanocomposite materials between inorganic glasses and organic polymers. *Adv Mater*. 1993;5:422–433.
6. Ou CF, Hsu MV. Preparation and characterization of cyclo olefin copolymer (COC)/silica nanoparticle composites by solution blending. *J Polym Res*. 2007;14:373–378.
7. Hong HY, Fu HP, Zhang YJ, Liu L, Wang J, Li HZ, Zheng Y. Surface-modified silica nanoparticles for reinforcement of PMMA. *J Appl Polym Sci*. 2007;105:2176–2184.
8. Acierno D, Filippone G, Romeo G, Russo P. Rheological aspects of PP-TiO2 micro and nanocomposites: a preliminary investigation. *Macromol Symp*. 2007;247:59–66.
9. Pluta M, Paul MA, Alexandre M, Dubois P. Plasticized polylactide/clay nanocomposites. I. The role of filler content and its surface organo-modification on the physico-chemical properties. *J Polym Sci Part B: Polym Phys*. 2006;44:299–311.
10. Yudin VE, Divoux GM, Otaigbe JU, Svetlichnyi VM. Synthesis and rheological properties of oligoimide/montmorillonite nanocomposites. *Polymer*. 2005;46:10866–10872.
11. Zhang H, Zhang Z, Friedrich K, Eger C. Property improvements of in situ epoxy nanocomposites with reduced interparticle distance at high nanosilica content. *Acta Mater*. 2006;54:1833–1842.
12. Muh E, Frey H, Klee JE, Mulhaupt RE. Organic-inorganic hybrid nanocomposites prepared by means of sol-gel condensation of bismethacrylatesilanes in reactive diluents. *Adv Funct Mater*. 2001;11:425–429.
13. Jain S, Goossens H, Picchioni F, Magusin P, Mezari B, Van Duin M. Synthetic aspects and characterization of polypropylenes-silica nanocomposites prepared via solid-state modification and sol-gel reactions. *Polymer*. 2005;46:6666–6681.
14. Dennis HR, Hunter DL, Chang SKD, White JL, Cho JW, Paul DR. Effect of melt processing conditions on the extent of exfoliation in organoclay-based nanocomposites. *Polymer*. 2001;41:9513–9522.
15. Vaia RA, Hope I, Giannelis EP. Synthesis and properties of two-dimensional nanostructures by direct intercalation of polymer melts in layered silicates. *Chem Mater*. 1993;5:1694–1696.
16. Vaia RA, Giannelis EP. Lattice model of polymer melt intercalation in organically-modified layered silicates. *Macromolecules*. 1997;30:7990–7999.
17. Vaia RA, Giannelis EP. Polymer melt intercalation in organically-modified layered silicates: model predictions and experiment. *Macromolecules*. 1997;30:8000–8009.
18. Liu L, Qi Z, Zhu XJ. Studies on nylon 6/clay nanocomposites by melt-intercalation process. *Appl Polym Sci*. 1999;71:1133.
19. Lertwimolnun W, Vergnes B. Effect of processing conditions on the formation of polypropylene/organoclay nanocomposites in a twin screw extruder. *Polym Eng Sci*. 2006;10:315–323.
20. Dou Q, Zhu X, Peter K, Demco DE, Moller M, Melian C. Preparation of polypropylene/silica composites by in-situ sol–gel processing using hyperbranched polyethoxysiloxane. *J Sol-Gel Sci Technol*. 2008;48:51–60.
21. Chen J, Chareonsak R, Puengpipat V, Marturunkakul S. Organic/inorganic composite materials for coating applications. *J Appl Polym Sci*. 1999;74:1341–1346.
22. Barlier V, Bounor-Legare V, Alcouffe P, Boiteux G, Davenas J. Formation of TiO2 domains in poly(9-vinylcarbazole) thin film by hydrolysis-condensation of a metal alkoxide. *Thin Solid Films*. 2007;16:6328–6331.
23. Barlier V, Bounor-Legaré V, Boiteux G, Davenas J, Leonard D. Hydrolysis-condensation reactions of titanium alkoxides in thin films: a study of the steric hindrance effect by X-ray photoelectron spectroscopy. *Appl Surf Sci*. 2008;17:5408–5412.
24. Xanthos M. *Reactive Extrusion: Principles and Practice*. Munich: Hanser, 1992.
25. Baker W, Scott C, Hu GH. *Reactive Polymer Blending*. Munich: Hanser, 2001.
26. Cassagnau P, Bounor-Legaré V, Fenouillot F. Reactive processing of thermoplastic polymers: a review of the fundamental aspects. *Int Polym Process*. 2007;22:218–258.
27. Vergnes B, Berzin F. Modelling of flow and chemistry in twin screw extruders. *Plast Rubber Compos Macromol Eng*. 2004;33: 409–415.
28. Jongbloed HA, Kiewiet JA, Van Dijk JH, Janssen LPBM. The self-wiping co-rotating twin-screw extruder as a polymerization reactor for methacrylates. *Polym Eng Sci*. 1995;35:1569–1579.
29. Vergnes B, Della Valle G, Delamare L. A global computer software for polymer flows in corotating twin screw extruders. *Polym Eng Sci*. 1998;38:1781–17929.
30. Carneiro OS, Covas JA, Vergnes B. Experimental and theoretical study of twin-screw extrusion of polypropylene. *J Appl Polym Sci*. 2000;78:1419–1430.
31. Delamare L, Vergnes B. Computation of the morphological changes of a polymer blend along a twin-extruder. *Polym Eng Sci*. 1996;36:1685–1693.

32. Lozano T, Lafleur PG, Grmela M, Vergnes B. Modeling filler dispersion along a twin screw extruder. *Int Polym Process*. 2003;18: 12–19.
33. Berzin F, Vergnes B, Dufossé P, Delamare L. Modelling of peroxide initiated controlled degradation of polypropylene in a twin screw extruder. *Polym Eng Sci*. 2000;40,344–356.
34. Poulesquen A, Vergnes B, Cassagnau P, Gimenez J, Michel A. Polymerization of ε-caprolactone in a twin screw extruder: experimental study. *Int Polym Process*. 2001;16:31–38.
35. Berzin F, Vergnes B. Transesterification of ethylene acetate copolymer in a twin screw extruder. *Int Polym Process*. 1998;13:13–22.
36. Berzin F, Tara A, Tighzert L, Vergnes B. Computation of starch cationization performances by twin screw extrusion. *Polym Eng Sci*. 2007;47:112–119.
37. Cassagnau P. Melt rheology of organo-clays and fumed silica nanocomposites. *Polymer*. 2008;49:2183–2196.
38. Yasuda KY, Amstrong RC, Cohen RE. Shear flow properties of concentrated solutions of linear and star branched polystyrenes. *Rheol Acta*. 1981;20:163–178.

Manuscript received Jan. 29, 2010, and revision received Aug. 4, 2010.